Second harmonic generation in the Weyl semimetal TaAs from a quantum kinetic equation

Zhi Li,[1] Ya-Qin Jin,[1] Takami Tohyama,[2] Toshiaki Iitaka,[3] Jiu-Xing Zhang,[1,*] and Haibin Su[4,5,†]
[1]*School of Materials Science and Engineering, Hefei University of Technology, Hefei 230009, Anhui, China*
[2]*Department of Applied Physics, Tokyo University of Science, Katsushika, Tokyo 125-8585, Japan*
[3]*Computational Astrophysics Laboratory, RIKEN, 2-1 Hirosawa, Wako, Saitama 351-0198, Japan*
[4]*Division of Materials Science, Nanyang Technological University, 50 Nanyang Avenue, 639798 Singapore*
[5]*Institute of Advanced Studies, Nanyang Technological University, 60 Nanyang View, 639673 Singapore*

(Received 29 September 2017; published 14 February 2018)

We classify the sources of second harmonic generation (SHG) of the Weyl semimetal TaAs by collisionless quantum kinetic equation into three kinds: i.e., injection current from the canonical band dispersion, shift current from a gauge invariant shift vector, and anomalous current from Berry curvature associated with the Fermi surface. Importantly, by using the realistic band model for TaAs, we predict that the SHG in TaAs is predominately contributed by the shift current, while the anomalous current has a minute contribution when the Weyl point is exactly located on the Fermi surface. Moreover, we highlight that the SHG contributed by the anomalous current decays fast with the increasing frequency of incident photons, and could be enhanced by proper electron or hole doping of TaAs.

DOI: 10.1103/PhysRevB.97.085201

I. INTRODUCTION

Dirac fermions in monolayer graphene featurelinear band dispersion near the Fermi level [1]. Consequently, monolayer graphene exhibits remarkably low absorption, $\sim$2.3%, of photons with wavelengths ranging from midinfrared to visible [2], and universal optical conductivity $\frac{e^2}{4\hbar}$ under high frequency optical field [3–6]. Due to the presence of spatial inversion symmetry, the second harmonic generation (SHG), i.e., nonlinear current with doubled frequency of incident photons, is absent in monolayer graphene, and only the strong third harmonic generation is reported [7]. Fortunately, Weyl semimetal materials with broken spatial inversion or time-reversal invariance (TRI) provide intrinsic sources leading to desirable SHG for nonlinear technology.

Weyl fermions are predicted in several magnetic materials with broken TRI, such as multilayer topological insulators [8], pyrochlore iridates $Y_2Ir_2O_7$ [9–12], ferromagnetic $HgCr_2Se_4$ and GdN [13–15], and magnetic half-Heusler $ZrCo_2Sn$ [16]. Interestingly, for nonmagnetic materials without spatial inversion symmetry, noncentrosymmetric transition metal diphosphides WTe_2 and $MoTe_2$ are also predicted to be Weyl semimetals with tilted Weyl cone [17–20]. The natures of the Weyl fermion and Fermi arc in WTe_2 and $MoTe_2$ are also supported by experimental measurements [21–26]. Particularly, the Weyl semimetallic phase has been theoretically predicted and experimentally verified in noncentrosymmetric transition metal monopnictides TaAs and TaP [27–34], which offers nice opportunity to study the detailed nonlinear processes in SHG.

The Weyl point or fermion with right (left)-handed chirality plays the role of monopole (antimonopole), which is the source (sink) of Berry curvature [35–37]. Under parallel magnetic and electric fields, a Weyl semimetal can present negative magnetoresistance resulting from a chiral anomaly [38,39]. Regarding the nonlinear optical (NLO) response in Weyl semimetals, SHG and photocurrent in TaAs were reported recently [40,41]. The SHG measurement showed that the dominating nonlinear coefficient d_{33} at wavelength $\lambda = 800$ nm is about 3600($\pm$550) pm/V, while the d_{15} and d_{31} are only about 3% of d_{33}. Significant photocurrent is also measured in TaAs under midinfrared polarized light with wavelength $\lambda = 10.6\ \mu$m. The photocurrent and SHG usually involve three different mechanisms, i.e., injection, shift, and anomalous currents [42–51]. The injection contribution is in the form of $j_I^{(2)} = \eta_{abc}(0;-\omega,\omega)E^b(\omega)E^c(\omega)$ and the tensor η_{abc} is asymmetric under indices b and c, and circularly polarized light is required to generate the injection current [42]. Similarly, the nonlinear anomalous current also requires circularly polarized light, and it is proportional to $\frac{1}{\omega^2}$, while ω is the frequency of incident photons [48–50]. The shift current results from the difference between intracell position matrices within valence and conduction bands [52]. Usually, broken spatial inversion symmetry is required for photocurrent and SHG in nonmagnetic materials. However, photocurrent and SHG can also be realized in magnetic materials with broken TRI, even though the spatial inversion symmetry is preserved [53–55].

Although the SHG in insulators is usually interpreted based on the mechanism of shift current [56–58], the mechanism of SHG in Weyl semimetals with zero band gap is still under investigation. For the Weyl semimetal TaAs, the mechanism of both the SHG and photocurrent was believed to be due to the shift vector [40,41,59]. Yet, detailed analysis of this interpretation is still absent. Besides, although SHG and photocurrent generated by the Berry curvature dipole were also predicted in Weyl semimetals with tilted Weyl fermions [45–48], the

*zjiuxing@hfut.edu.cn
†hbsu@ntu.edu.sg

Berry curvature induced SHG has not been identified in Weyl semimetal TaAs with minute tilted Weyl fermions, even though the chirality of Weyl fermions in TaAs is demonstrated by the photocurrent experiment [41]. Therefore, clarification of the Berry curvature dipole's contribution to SHG in TaAs is needed. In this work, we investigate SHG of Weyl semimetals by a collisionless quantum kinetic equation and identify three types of courses for generating SHG, i.e., injection current from the parabolic band dispersion, shift current from a gauge invariant shift vector, and anomalous current from Berry curvature on the Fermi surface. Using the realistic band model for TaAs, we predict that the SHG is predominately from the shift current, while contributions from both injection and anomalous currents are less pronounced. Importantly, the SHG contributed from anomalous current decays faster with the increasing frequency of incident photons, and proper electron or hole doping could deliberately enhance SHG through anomalous current.

II. SHG FROM A QUANTUM KINETIC EQUATION

Under an external electric field, light-matter coupling can be described by a model Hamiltonian in length gauge [42,50,51],

$$H(\mathbf{k},t) = h_0(\mathbf{k}) + H_1 = h_0(\mathbf{k}) - e\mathbf{r}\cdot E(t), \tag{1}$$

where $h_0(\mathbf{k})$ is the momentum dependent unperturbed Hamiltonian, and $E(t) = E(\omega)e^{-i\omega t}$ is a time-dependent external electric field. For intrinsic NLO effect from band structure, we ignore all the scattering terms here. With orthogonal Bloch wave functions $|n\rangle = e_n(\mathbf{k},\mathbf{r})$ satisfying $h_0(\mathbf{k})e_n(\mathbf{k}) = \epsilon_n e_n(\mathbf{k})$, the solution for Hamiltonian (1) can be expressed as

$$|\psi(\mathbf{r})\rangle = \int_{BZ} \frac{d^3\mathbf{k}}{(2\pi)^3} a_n(\mathbf{k}) e_n(\mathbf{k},\mathbf{r}), \tag{2}$$

where n is the band index, and momentum takes values in the whole Brillouin zone (BZ). The density matrix ρ is defined as

$$\rho(\mathbf{k}) = a_n^*(\mathbf{k}) a_m(\mathbf{k}) |e_n\rangle\langle e_m|. \tag{3}$$

The dynamics of $\rho(\mathbf{k},t)$ can be described by a collisionless quantum kinetic equation [60,61],

$$-\hbar\frac{\partial\rho(\mathbf{k},t)}{\partial t} = e\mathbf{E}\cdot\frac{\partial\rho(\mathbf{k},t)}{\partial\mathbf{k}} + i[H,\rho(\mathbf{k},t)]. \tag{4}$$

By perturbation calculation, the linear order of ρ reads

$$\begin{aligned}\rho^{(1)}_{nn}(\mathbf{k},\omega) &= \frac{-ie\mathbf{E}(\omega)}{\hbar\omega}\cdot\frac{\partial\rho^{(0)}_{nn}(\mathbf{k})}{\partial\mathbf{k}} \\ &= \frac{-ie\mathbf{E}(\omega)}{\hbar\omega}\cdot\frac{\partial\epsilon_n(\mathbf{k})}{\partial\mathbf{k}}\delta(\mathbf{k}-k_F)\end{aligned} \tag{5}$$

for the intraband density matrix. Here, $\rho^{(0)}_{nn}$ is the Fermi distribution function $1/[1+\exp(\frac{\epsilon_n-\mu}{k_BT})]$ (μ, k_B, T are Fermi energy, Boltzmann constant, and temperature, respectively) of the unperturbed ground state, and $\frac{\partial\rho^{(0)}_{nn}(\mathbf{k})}{\partial\epsilon_n(\mathbf{k})} = \delta(\mathbf{k}-k_F)$ at 0 K, which is nonzero only on the Fermi surface. We also assumed that Fermi energy μ is independent of temperature T for simplicity. The first order of the interband ($n \neq m$) density matrix reads

$$\rho^{(1)}_{nm}(\mathbf{k},\omega) = \frac{\langle n|H_1|m\rangle\left(\rho^{(0)}_{mm}(\mathbf{k}) - \rho^{(0)}_{nn}(\mathbf{k})\right)}{\hbar\omega - \epsilon_{nm}}, \tag{6}$$

where $\epsilon_{nm} = \epsilon_n(\mathbf{k}) - \epsilon_m(\mathbf{k})$. The linear current along the y direction can be determined by

$$J^{(1)}_y(\omega) = -e\sum_n \int_{BZ}\frac{d\mathbf{k}}{(2\pi)^3}\langle n|\rho^{(1)}(\mathbf{k},\omega)v_0(\mathbf{k})|n\rangle. \tag{7}$$

Here, the intraband velocity [62] is defined as

$$\langle n|v_0|n\rangle = \langle n|\frac{\partial h_0(\mathbf{k})}{\hbar\partial\mathbf{k}}|n\rangle = \frac{\partial\epsilon_n}{\hbar\partial\mathbf{k}}, \tag{8}$$

and the interband velocity is defined as

$$\langle n|v_0|m\rangle = \langle n|\frac{\partial h_0(\mathbf{k})}{\hbar\partial\mathbf{k}}|m\rangle = \frac{\epsilon_{mn}}{\hbar}\langle n|\partial_{\mathbf{k}}|m\rangle. \tag{9}$$

Assuming the external electric field is along the x direction, the intraband linear current from Drude conductivity reads

$$\begin{aligned}J^{(1)}_{D,x}(\omega) &= -\frac{e}{\hbar}\sum_n\int_{BZ}\frac{d\mathbf{k}}{(2\pi)^3}\rho^{(1)}_{nn}(\mathbf{k})\frac{\partial\epsilon_n(\mathbf{k})}{\partial k_x} \\ &= -\frac{ie^2E_x(\omega)}{\hbar^2\omega}\sum_n\int_{FS}\frac{d\mathbf{k}}{(2\pi)^2}\left(\frac{\partial\epsilon_n(\mathbf{k})}{\partial k_x}\right)^2,\end{aligned} \tag{10}$$

where we make use of the equation $\frac{\partial\rho^{(0)}_{nn}(\mathbf{k})}{\partial\epsilon_n(\mathbf{k})} = \delta(\mathbf{k}-k_F)$ and k_F is the Fermi vector. The interband linear current along the y direction reads

$$\begin{aligned}J^{(1)}_{I,y}(\omega) &= i\frac{e^2}{\hbar}E_x(\omega)\sum_{n\neq m}\int_{BZ}\frac{d\mathbf{k}}{(2\pi)^3}\epsilon_{nm}\frac{2A\hbar\omega\rho^{(0)}_{nn}(\mathbf{k})}{(\hbar\omega)^2-\epsilon^2_{nm}} \\ &\quad -\frac{e^2}{\hbar}E_x(\omega)\sum_{n\neq m}\int_{BZ}\frac{d\mathbf{k}}{(2\pi)^3}\frac{2B\rho^{(0)}_{nn}(\mathbf{k})\epsilon^2_{nm}}{(\hbar\omega)^2-\epsilon^2_{nm}},\end{aligned} \tag{11}$$

where functions A and B are defined as

$$2A = \langle\partial_x n|m\rangle\langle m|\partial_y n\rangle + \langle\partial_y n|m\rangle\langle m|\partial_x n\rangle, \tag{12}$$

$$-2B = i\langle\partial_x n|m\rangle\langle m|\partial_y n\rangle - i\langle\partial_y n|m\rangle\langle m|\partial_x n\rangle. \tag{13}$$

In the derivation of Eq. (11), we make use of the interband position matrix [63,64], i.e., the interband Berry connection,

$$\langle n|\mathbf{r}|m\rangle = i\langle n|\partial_{\mathbf{k}}|m\rangle = \mathbf{a}_{nm}. \tag{14}$$

For an applied static external field to the gapped system, the first term in Eq. (11) vanishes, and the transverse Hall current reads

$$\begin{aligned}J^{(1)}_{I,y} &= -\frac{e^2}{\hbar}E_x\sum_n\int_{BZ}\frac{d\mathbf{k}}{(2\pi)^3}(-2B) \\ &= -\frac{e^2}{\hbar}E_x\sum_n\int_{BZ}\frac{d\mathbf{k}}{(2\pi)^3}\nabla\times\mathbf{a}_{nn}(\mathbf{k}).\end{aligned} \tag{15}$$

The Hall conductivity from each band is $\frac{e^2}{\hbar}\int\frac{dk}{(2\pi)^2}\nabla\times a_{nn}$ for a two-dimensional system, i.e., the Chern number.

With an applied external field along direction x, the second-order density matrix $\rho^{(2)}(t) \propto E^2$, and the intraband and

interband density matrices read

$$\rho_{nn}^{(2)}(2\omega) = -\frac{[eE_x(\omega)]^2}{2(\hbar\omega)^2}\partial_x^2\rho_{nn}^{(0)}(\mathbf{k}) + \sum_m \frac{\langle n|H_1|m\rangle\rho_{mn}^{(1)} - \rho_{nm}^{(1)}\langle m|H_1|n\rangle}{2\hbar\omega}, \tag{16}$$

$$\rho_{nm}^{(2)}(2\omega) = \frac{-ieE(\omega)}{2\hbar\omega - \epsilon_{nm}}\left(\frac{\partial}{\partial k} + i[\mathbf{a}_{mm} - \mathbf{a}_{nn}]\right)\rho_{nm}^{(1)} + \frac{\langle n|H_1|m\rangle\left(\rho_{mm}^{(1)} - \rho_{nn}^{(1)}\right)}{2\hbar\omega - \epsilon_{nm}} + \sum_{l\neq n, l\neq m}\frac{\langle n|H_1|l\rangle\rho_{lm}^{(1)} - \rho_{nl}^{(1)}\langle l|H_1|m\rangle}{2\hbar\omega - \epsilon_{nm}}, \tag{17}$$

respectively. The second-order current is determined by

$$J_y^{(2)} = \sum_n \langle n|v_0\rho^{(2)}|n\rangle = \sum_{nl}\langle n|v_0|l\rangle\langle l|\rho^{(2)}|n\rangle. \tag{18}$$

For $n = l$, the intraband current $J_{inj}^{(2)}(2\omega)$ along the y direction reads

$$J_{inj}^{(2)}(2\omega) = \frac{e}{\hbar}\frac{[eE_x(\omega)]^2}{2(\hbar\omega)^2}\sum_n\int_{BZ}\frac{d\mathbf{k}}{(2\pi)^3}\partial_x^2\rho_{nn}^{(0)}(k)\frac{\partial\epsilon_n(k)}{\partial k_y} - \frac{e}{\hbar}\sum_{n\neq m}\int_{BZ}\frac{d\mathbf{k}}{(2\pi)^3}\frac{\langle n|H_1m\rangle\langle m|H_1|n\rangle}{(\hbar\omega)^2 - \epsilon_{nm}^2}\rho_{nn}^{(0)}(k)\frac{\partial\epsilon_{nm}}{\partial k_y}. \tag{19}$$

Since the integrand is proportional to $\frac{\partial\epsilon(\mathbf{k})}{\partial\mathbf{k}}$, $J_{inj}^{(2)}(2\omega)$ is dubbed an injection current. For $n \neq l$, we have three additional types of nonlinear current from different mechanisms in Eq. (18). Here, we ignore the nonlinear current from the third term in Eq. (17), which involves three bands. The other two types of nonlinear current with doubled frequency of incident photon read

$$J_{S+A,y}^{(2)} = \frac{e}{\hbar}\sum_{nm}\int_{BZ}\frac{d\mathbf{k}}{(2\pi)^3}\frac{ieE(\omega)\langle m|\partial_y h_0|n\rangle}{2\hbar\omega - \epsilon_{nm}}\mathbf{D}_{nm}\rho_{nm}^{(1)} - \frac{e}{\hbar}\sum_{n\neq m}\int_{BZ}\frac{d\mathbf{k}}{(2\pi)^3}\frac{\langle n|\partial_y m\rangle\langle m|H_1|n\rangle\left(\rho_{nn}^{(1)} - \rho_{mm}^{(1)}\right)}{2\hbar\omega + \epsilon_{nm}}. \tag{20}$$

The first term in Eq. (20) is the shift current resulting from shift vector $\mathbf{D}_{nm}(k) = \frac{\partial}{\partial\mathbf{k}} + i[\mathbf{a}_{mm} - \mathbf{a}_{nn}]$, which characterizes the difference between intracell position matrices within valence and conduction bands [37,65]. The shift current is gauge invariant, i.e., invariant under local phase transformation of the wave function. The second term in Eq. (20) is the anomaly current from Berry curvature. With the definitions of A and B in Eqs. (12) and (13), respectively, the anomalous current reads

$$J_{A,y}^{(2)}(2\omega) = \frac{ie^2E_x(\omega)}{\hbar}\sum_{n\neq m}\int_{BZ}\frac{d\mathbf{k}}{(2\pi)^3}\epsilon_{nm}\frac{4A\hbar\omega}{(2\hbar\omega)^2 - \epsilon_{nm}^2}\rho_{nn}^{(1)}(k) - \frac{e^2}{\hbar}E_x\sum_{n\neq m}\int_{BZ}\frac{d\mathbf{k}}{(2\pi)^3}\frac{2B\epsilon_{nm}^2}{(2\hbar\omega)^2 - \epsilon_{nm}^2}\rho_{nn}^{(1)}(k). \tag{21}$$

The SHG from the injection, shift, and anomaly current can be easily calculated by

$$\chi_{yxx}^{(2)}(2\omega;\omega,\omega) = \frac{\sigma_{yxx}^{(2)}(2\omega;\omega,\omega)}{2i\omega\varepsilon_0}, \tag{22}$$

where ε_0 is vacuum permittivity. The nonlinear optic conductivity $\sigma_{yxx}^{(2)}(2\omega;\omega,\omega)$ reads

$$\sigma_{yxx}^{(2)}(2\omega;\omega,\omega) = \frac{J_y^{(2)}(2\omega;\omega,\omega)}{E_xE_x}, \tag{23}$$

and $J_y^{(2)}(2\omega;\omega,\omega)$ can be injection, shift, and anomaly current.

III. BAND MODEL CALCULATION

For a Weyl semimetal, the low energy band dispersion near the Fermi level usually can be described by a minimal Hamiltonian [66]. For the Weyl semimetal TaAs, there are only four bands near the the Fermi level in the calculated band structure by first-principles calculation [27]. The low energy electronic structure near the Fermi level can be described by

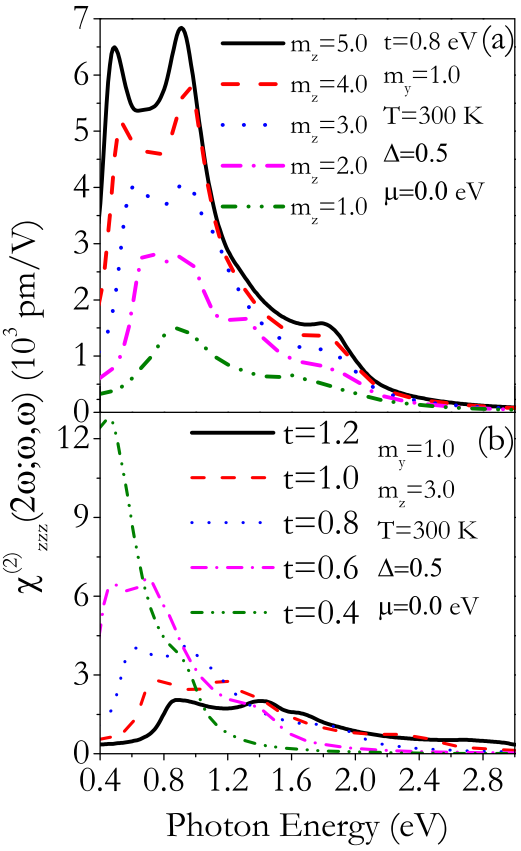

FIG. 1. Calculated parameters m_z (a) and t (b) dependent SHG coefficients $\chi_{zzz}^{(2)}(2\omega;\omega,\omega)$ contributed from shift current.

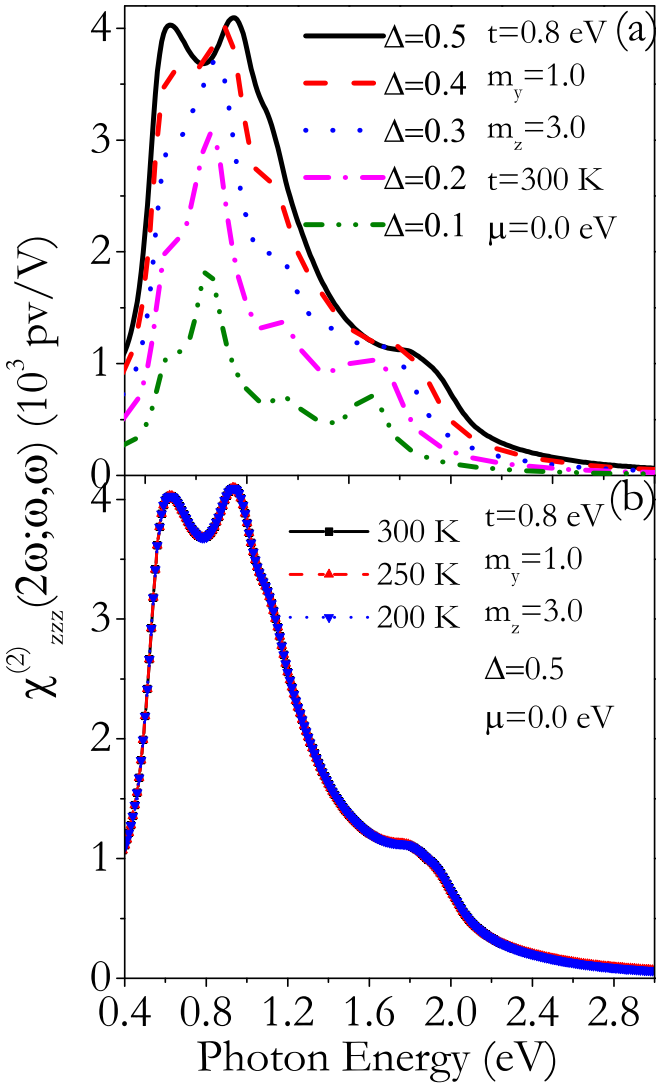

FIG. 2. Calculated parameter Δ (a) and temperature T (b) dependent SHG coefficients $\chi^{(2)}_{zzz}(2\omega;\omega,\omega)$ contributed from shift current.

the following minimal model preserving TRI:

$$h_0(\mathbf{k}) = t[\cos k_x + m_y(1-\cos k_y) + m_z(1-\cos k_z)]\sigma_x + t[\sin k_y + \Delta\cos k_y s_x]\sigma_y + t\sin k_z s_x \sigma_z, \quad (24)$$

as introduced by Wu *et al.* [40]. In concrete material TaAs, there are some bands far away from the Fermi level. However, these bands can only contribute to SHG by the mechanism of shift current as in the case of most insulators, if we exclude the four bands near the Fermi level [56]. Therefore, those bands far away from the Fermi level are not taken into the calculation for simplicity. Here, σ_i and s_i are standard Pauli matrices acting on the orbital and spin degrees of freedom, respectively. The spatial inversion symmetry is broken by parameter Δ. The bandwidth is determined by parameters t, m_y, and m_z. This model Hamiltonian preserves the $mm2$ point group, which is a subgroup of $4mm$ point group of TaAs. This Hamiltonian renders four Weyl points with linear band dispersion on the Fermi level. Because of nonzero parameter m_y, the band dispersion is neither an odd nor an even function of momentum

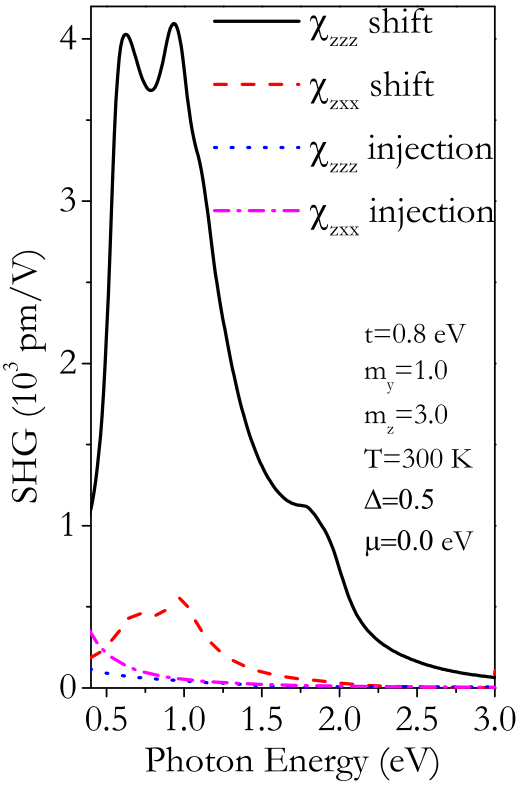

FIG. 3. Calculated photon energy dependent SHG contributed from shift current and injection current with parameters $t = 0.8$ eV, $\Delta = 0.5$, $m_y = 1.0$, $m_z = 3.0$, $T = 300$ K, and $\mu = 0.0$ eV.

$\mathbf{k}$, which takes values the in whole Brillouin zone. With the model Hamiltonian (24), the calculated parameters m_z and t dependent SHG coefficients $\chi^{(2)}_{zzz}(2\omega;\omega,\omega)$ contributed from shift current by Eq. (20) are shown in Fig. 1. The maximal value in each curve is increasing (decreasing) with the increase of parameter m_z (t). Especially, when m_z is larger than 3.0, there exists an obvious dip in the curve around photon energy 0.7 eV. The dip in the curve can be interpreted by the enhanced anisotropy of electronic structure resulting from relatively large m_z. The calculated parameter Δ dependent $\chi^{(2)}_{zzz}(2\omega;\omega,\omega)$ contributed from shift current is shown in Fig. 2(a), and it reveals that $\chi^{(2)}_{zzz}(2\omega;\omega,\omega)$ is decreasing with the decrease of parameter Δ. In Fig. 2(b), we show the temperature dependent $\chi^{(2)}_{zzz}(2\omega;\omega,\omega)$, indicating that the dependence between temperature and $\chi^{(2)}_{zzz}(2\omega;\omega,\omega)$ is very weak. Numerical calculation also reveals that $\chi^{(2)}_{zxx}(2\omega;\omega,\omega)$ contributed from shift current is also weakly dependent on temperature (not shown).

With parameters $\Delta = 0.5$, $m_z = 3.0$, and $t = 0.8$ eV, the calculated SHG coefficient $\chi^{(2)}_{zzz}(2\omega;\omega,\omega) = 2d_{33}$ contributed by shift current at photon energy $\hbar\omega = 1.55$ eV, i.e., wavelength 800 nm, is roughly 1/6 of the experimental result $d_{33} = 3600(\pm 550)$ pm/V [40]. Since Eq. (24) only renders four Weyl points, i.e., 1/6 of the Weyl points in concrete TaAs, we adopt $\Delta = 0.5$, $m_z = 3.0$, and $t = 0.8$ eV in our following calculation. These parameters take the same values as those adopted in Ref. [40], except m_z. The calculated photon energy dependent SHG coefficients $\chi^{(2)}_{zzz}(2\omega;\omega,\omega) = 2d_{33}$ and $\chi^{(2)}_{zxx}(2\omega;\omega,\omega) = 2d_{31}$ contributed from injection current and shift current are shown in Fig. 3. The calculated

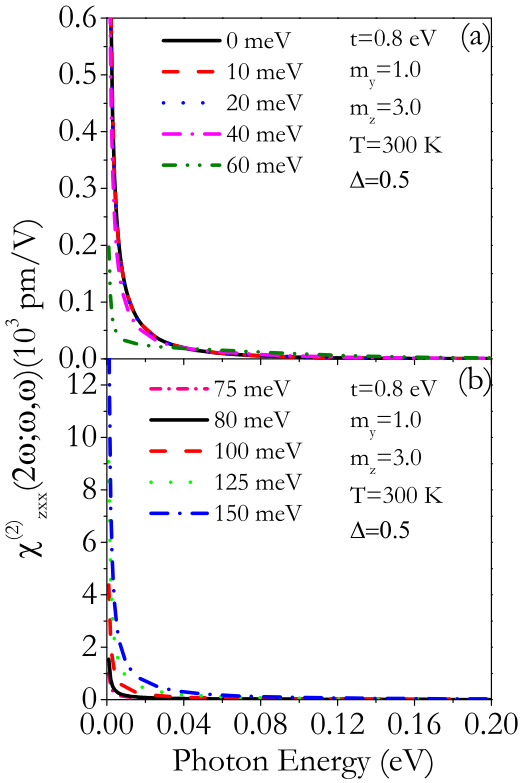

FIG. 4. Calculated Fermi energy dependent SHG coefficients $\chi^{(2)}_{zxx}(2\omega;\omega,\omega)$ contributed by anomalous current with parameters $t = 0.8$ eV, $\Delta = 0.5$, $m_y = 1.0$, $m_z = 3.0$, and $T = 300$ K, for Fermi energy $\mu \leqslant 60$ meV (a) and $\mu \geqslant 75$ meV (b).

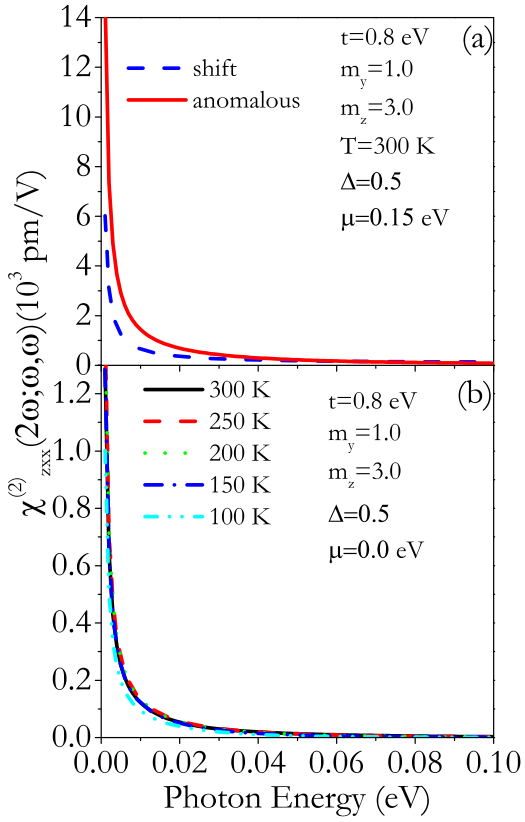

FIG. 5. Calculated photon energy dependent SHG coefficients $\chi^{(2)}_{zxx}(2\omega;\omega,\omega)$ contributed by anomalous and shift currents (a) when $\mu = 0.15$ eV, and temperature dependent SHG coefficients $\chi^{(2)}_{zxx}(2\omega;\omega,\omega)$ induced by anomalous current (b).

SHG coefficient d_{33} contributed by injection current at 800 nm is much smaller than the SHG coefficient contributed by shift current. At 800 nm, the calculated SHG coefficient d_{31} contributed by either injection or shift current is much smaller than the SHG d_{33} contributed by shift current. These calculated results present the main salient features of the experimental measurements.

Since $\rho^{(1)}_{nn}(\mathbf{k})$ is proportional to $\delta(\mathbf{k} - k_F)$, Eq. (21) indicates that the anomalous current is mainly determined by the states at the Fermi level. In the band structure of an ideal Weyl semimetal, the Weyl point is exactly on the Fermi level, and $\rho^{(1)}_{nn}(\mathbf{k}_F)$ is finite at 0 K. The calculated Fermi energy dependent SHG coefficient $\chi^{(2)}_{zxx}(2\omega;\omega,\omega)$ induced by anomalous current is shown in Fig. 4. When the Fermi level $\mu \leqslant 60$ meV, the SHG coefficient $\chi^{(2)}_{zxx}(2\omega;\omega,\omega)$ at low frequency is decreasing with the increase of Fermi energy, i.e., SHG induced by anomalous current is decreasing when the Fermi level moves far away from the Weyl point. Overall, the $\chi^{(2)}_{zxx}(2\omega;\omega,\omega)$ induced by anomalous current is minute when the Fermi level $\mu \leqslant 60$ meV. However, with the further increase of Fermi energy, $\chi^{(2)}_{zxx}(2\omega;\omega,\omega)$ increases with the Fermi energy, as shown in Fig. 4(b). When $\mu \geqslant 75$ meV, the increase of $\chi^{(2)}_{zxx}(2\omega;\omega,\omega)$ with increasing Fermi energy is not related to the anomalous current from the linear band dispersion near the Weyl point. The increasing SHG is obviously related to the anomalous current from parabolic band dispersion at high energy [51], since the low energy part near the Weyl point is occupied and the transition between the upper part and lower part of the Weyl point is forbidden. It is revealed by Fig. 4 that the $\chi^{(2)}_{zxx}(2\omega;\omega,\omega)$ induced by anomalous current can be enhanced by electron or hole doping into TaAs. With varying parameters t, Δ, and m_z, we checked the enhancement of $\chi^{(2)}_{zxx}(2\omega;\omega,\omega)$ by electron or hole doping. We concluded that the enhancement of $\chi^{(2)}_{zxx}(2\omega;\omega,\omega)$ by doping is robust, even though different parameters are adopted. Especially, when the Fermi level is rather far away from the Weyl point, the energy difference at the Fermi vector $\epsilon_{nm}(k_F)$ should be rather large. In the case of low frequency $\omega \ll \mu$, where μ is the Fermi level measured from Weyl point, the first term in Eq. (21) can be ignored, and the anomalous current reads

$$J^{(2)}_{A,y}(2\omega) = -\frac{ie^3}{\hbar^2\omega} E_x^2(\omega) \sum_n \int_{FS} d^2k \frac{\partial \epsilon_n(\mathbf{k})}{\partial k_x} \Omega(\mathbf{k}), \quad (25)$$

where the Berry curvature Ω reads

$$\Omega(\mathbf{k}) = \nabla \times \mathbf{a}_{nn} = i\langle u_n|\partial_k|u_n\rangle. \quad (26)$$

From Eqs. (22) and (23), the SHG from anomalous current should be inversely proportional to $1/\omega^2$ in the case of $\omega \ll \mu$. Indeed, regardless of the concentration of doping, the calculated results show that the SHG coefficient decays more quickly with the increasing frequency of incident photons, as shown in Fig. 4.

The calculated $\chi^{(2)}_{zxx}(2\omega;\omega,\omega)$ induced by injection current is much larger than that induced by anomalous current when

the Weyl point is exactly on the Fermi level. However, when the Fermi energy is 0.15 eV above the Weyl points, the calculated SHG coefficient $\chi^{(2)}_{zxx}(2\omega;\omega,\omega)$ contributed by anomalous current is larger than that contributed from shift current when the frequency of incident photons is very low, as shown in Fig. 5(a). The SHG contributed by shift current is not monotonically decreasing with the increase of photon energy (not shown), while the SHG contributed by anomalous current is monotonically decreasing.

The temperature dependent $\chi^{(2)}_{zxx}(2\omega;\omega,\omega)$ induced by anomalous current is shown in Fig. 5(b), and it reveals that dependence between temperature and $\chi^{(2)}_{zxx}(2\omega;\omega,\omega)$ is very weak. With the increase of temperature, $\chi^{(2)}_{zxx}(2\omega;\omega,\omega)$ is slightly increasing, i.e., the anomalous current is enhanced by high temperature. However, the increase of $\chi^{(2)}_{zxx}(2\omega;\omega,\omega)$ is not monotonic with the increase of temperature. When the temperature is higher than 250 K, $\chi^{(2)}_{zxx}(2\omega;\omega,\omega)$ decreases with the increase of temperature.

IV. SUMMARY

The sources of SHG of Weyl semimetals are analyzed by a collisionless quantum kinetic equation in this work. Three types of sources are injection current from the band dispersion, shift current from gauge invariant shift vector, and anomalous current from Berry curvature on the Fermi surface. Clearly, SHG is mainly generated by the shift current mechanism in TaAs, while the anomalous current is less pronounced when the Weyl point is on the Fermi surface. Additionally, we predicted that SHG contributed by the anomalous current decays faster with the increasing of frequency of incident photons, which can be enhanced by properly doping electrons or holes into TaAs.

ACKNOWLEDGMENTS

This work was supported by the National Natural Science Foundation of China (Grants No. 11604068 and No. 51371010) and the Fundamental Research Funds for the Central Universities. T.T. and T.I. are supported by MEXT via "Exploratory Challenge on Post-K Computer" (Frontiers of Basic Science: Challenging the Limits). The calculations were performed on the Hokusai system (Project No. Q17231,G17036) of Riken. H.B.S. is grateful for support from the Society of Interdisciplinary Research (SOIREE).

[1] A. H. Castro Neto, F. Guinea, N. M. R. Peres, K. S. Novoselov, and A. K. Geim, Rev. Mod. Phys. **81**, 109 (2009).
[2] R. R. Nair, P. Blake, A. N. Grigorenko, K. S. Novoselov, T. J. Booth, T. Stauber, N. M. R. Peres, and A. K. Geim, Science **320**, 1308 (2008).
[3] K. F. Mak, M. Y. Sfeir, Y. Wu, C. H. Lui, J. A. Misewich, and T. F. Heinz, Phys. Rev. Lett. **101**, 196405 (2008).
[4] V. P. Gusynin, S. G. sharapov, and J. P. Carbotte, Int. J. Mod. Phys. B **21**, 4611 (2007).
[5] T. Ando, Y. Zheng, and H. Suzuura, J. Phys. Soc. Jpn. **71**, 1318 (2002).
[6] H. Min and A. H. MacDonald, Phys. Rev. Lett. **103**, 067402 (2009).
[7] S.-Y. Hong, J. I. Dadap, N. Petrone, P.-C. Yeh, J. Hone, and R. M. Osgood, Jr., Phys. Rev. X **3**, 021014 (2013).
[8] A. A. Burkov and L. Balents, Phys. Rev. Lett. **107**, 127205 (2011).
[9] X. Wan, A. M. Turner, A. Vishwanath, and S. Y. Savrasov, Phys. Rev. B **83**, 205101 (2011).
[10] K.-Y. Yang, Y.-M. Lu, and Y. Ran, Phys. Rev. B **84**, 075129 (2011).
[11] T. Bzdušek, A. Rüegg, and M. Sigrist, Phys. Rev. B **91**, 165105 (2015).
[12] Y. Du, B. Wan, D. Wang, L. Sheng, C.-G. Duan, and X. Wan, Sci. Rep. **5**, 14423 (2015).
[13] G. Xu, H. Weng, Z. Wang, X. Dai, and Z. Fang, Phys. Rev. Lett. **107**, 186806 (2011).
[14] Z. Li, J. Kim, N. Kioussis, S.-Y. Ning, H. Su, T. Iitaka, T. Tohyama, X. Yang, and J.-X. Zhang, Phys. Rev. B **92**, 201303(R) (2015).
[15] Z. Li, D.-D. Xu, S.-Y. Ning, H. Su, T. Iitaka, T. Tohyama, and J.-X. Zhang, Int. J. Mod. Phys. B **31**, 1750217 (2017).
[16] Z. Wang, M. G. Vergniory, S. Kushwaha, M. Hirschberger, E. V. Chulkov, A. Ernst, N. P. Ong, R. J. Cava, and B. A. Bernevig, Phys. Rev. Lett. **117**, 236401 (2016).
[17] A. A. Soluyanov, D. Gresch, Z. Wang, Q. Wu, M. Troyer, X. Dai, and B. A. Bernevig, Nature (London) **527**, 495 (2015).
[18] Z. Wang, D. Gresch, A. A. Soluyanov, W. Xie, S. Kushwaha, X. Dai, M. Troyer, R. J. Cava, and B. A. Bernevig, Phys. Rev. Lett. **117**, 056805 (2016).
[19] Y. Sun, S.-C. Wu, M. N. Ali, C. Felser, and B. Yan, Phys. Rev. B **92**, 161107(R) (2015).
[20] T.-R. Chang *et al.*, Nat. Commun. **7**, 10639 (2016).
[21] A. Tamai, Q. S. Wu, I. Cucchi, F. Y. Bruno, S. Riccò, T. K. Kim, M. Hoesch, C. Barreteau, E. Giannini, C. Besnard, A. A. Soluyanov, and F. Baumberger, Phys. Rev. X **6**, 031021 (2016).
[22] C. Wang, Y. Zhang, J. Huang, S. Nie, G. Liu, A. Liang, Y. Zhang, B. Shen, J. Liu, C. Hu, Y. Ding, D. Liu, Y. Hu, S. He, L. Zhao, L. Yu, J. Hu, J. Wei, Z. Mao, Y. Shi, X. Jia, F. Zhang, S. Zhang, F. Yang, Z. Wang, Q. Peng, H. Weng, X. Dai, Z. Fang, Z. Xu, C. Chen, and X. J. Zhou, Phys. Rev. B **94**, 241119(R) (2016).
[23] I. Belopolski *et al.*, Nat. Commun. **7**, 13643 (2016).
[24] Y. Wu, D. Mou, N. H. Jo, K. Sun, L. Huang, S. L. Bud'ko, P. C. Canfield, and A. Kaminski, Phys. Rev. B **94**, 121113(R) (2016).
[25] K. Deng *et al.*, Nat. Phys. **12**, 1105 (2016).
[26] L. Huang, T. M. McCormick, M. Ochi, Z. Zhao, M.-T. Suzuki, R. Arita, Y. Wu, D. Mou, H. Cao, J. Yan, N. Trivedi, and A. Kaminski, Nat. Mater. **15**, 1155 (2016).
[27] H. Weng, C. Fang, Z. Fang, B. A. Bernevig, and X. Dai, Phys. Rev. X **5**, 011029 (2015).
[28] Y. Sun, Y. Zhang, C. Felser, and B. Yan, Phys. Rev. Lett. **117**, 146403 (2016).
[29] B. Q. Lv, H. M. Weng, B. B. Fu, X. P. Wang, H. Miao, J. Ma, P. Richard, X. C. Huang, L. X. Zhao, G. F. Chen, Z. Fang, X. Dai, T. Qian, and H. Ding, Phys. Rev. X **5**, 031013 (2015).

[30] B. Q. Lv, N. Xu, H. M. Weng, J. Z. Ma, P. Richard, X. C. Huang, L. X. Zhao, G. F. Chen, C. E. Matt, F. Bisti, V. N. Strocov, J. Mesot, Z. Fang, X. Dai, T. Qian, M. Shi, and H. Ding, Nat. Phys. **11**, 724 (2015).
[31] L. X. Yang, Z. K. Liu, Y. Sun, H. Peng, H. F. Yang, T. Zhang, B. Zhou, Y. Zhang, Y. F. Guo, M. Rahn, D. Prabhakaran, Z. Hussain, S.-K. Mo, C. Felser, B. Yan, and Y. L. Chen, Nat. Phys. **11**, 728 (2015).
[32] Su-Yang Xu *et al.*, Phys. Rev. Lett. **116**, 096801 (2016).
[33] F. Arnold, M. Naumann, S.-C. Wu, Y. Sun, M. Schmidt, H. Borrmann, C. Felser, B. Yan, and E. Hassinger, Phys. Rev. Lett. **117**, 146401 (2016).
[34] Z. K. Liu, L. X. Yang, Y. Sun, T. Zhang, H. Peng, H. F. Yang, C. Chen, Y. Zhang, Y. F. Guo, D. Prabhakaran, M. Schmidt, Z. Hussain, S.-K. Mo, C. Felser, B. Yan, and Y. L. Chen, Nat. Mater. **15**, 27 (2016).
[35] A. A. Burkov, Annu. Rev. Condens. Matter Phys. **9**, 359 (2018).
[36] E. Witten, La Rivista del Nuovo Cimento **39**, 313 (2016).
[37] N. P. Armitage, E. J. Mele, and A. Vishwanath, Rev. Mod. Phys. **90**, 15001 (2018).
[38] D. T. Son, and B. Z. Spivak, Phys. Rev. B **88**, 104412 (2013).
[39] A. A. Burkov, Phys. Rev. B **91**, 245157 (2015).
[40] L. Wu, S. Patankar, T. Morimoto, N. L. Nair, E. Thewalt, A. Little, J. G. Analytis, J. E. Moore, and J. Orenstein, Nat. Phys. **13**, 350 (2017).
[41] Q. Ma, S.-Y. Xu, C.-K. Chan, C.-L. Zhang, G. Chang, Y. Lin, W. Xie, T. Palacios, H. Lin, S. Jia, P. A. Lee, P. Jarillo-Herrero, and N. Gedik, Nat. Phys. **13**, 842 (2017).
[42] J. E. Sipe and A. I. Shkrebtii, Phys. Rev. B **61**, 5337 (2000).
[43] E. Deyo, L. E. Golub, E. L. Ivchenko, and B. Spivak, arXiv:0904.1917.
[44] Y. Gao, S. A. Yang, and Q. Niu, Phys. Rev. Lett. **112**, 166601 (2014).
[45] L. E. Golub, E. L. Ivchenko, and B. Z. Spivak, JETP Lett. **105**, 782 (2017).
[46] E. J. König, H.-Y. Xie, D. A. Pesin, and A. Levchenko, Phys. Rev. B **96**, 075123 (2017).
[47] Y. Zhang, Y. Sun, and B. Yan, Phys. Rev. B **97**, 041101 (2018).
[48] I. Sodemann and L. Fu, Phys. Rev. Lett. **115**, 216806 (2015).
[49] T. Morimoto, S. Zhong, J. Orenstein, and J. E. Moore, Phys. Rev. B **94**, 245121 (2016).
[50] H. Rostami and M. Polini, arXiv:1705.09915.
[51] A. Cortijo, Phys. Rev. B **94**, 235123 (2016).
[52] T. Morimoto and N. Nagaosa, Sci. Adv. **2**, e1501524 (2016).
[53] A. A. Zyuzin and A. Yu. Zyuzin, Phys. Rev. B **95**, 085127 (2017).
[54] B. Kaminski, M. Lafrentz, R. V. Pisarev, D. R. Yakovlev, V. V. Pavlov, V. A. Lukoshkin, A. B. Henriques, G. Springholz, G. Bauer, E. Abramof, P. H. O. Rappl, and M. Bayer, Phys. Rev. B **81**, 155201 (2010).
[55] M. Fiebig, D. Fröhlich, Th. Lottermoser, V. V. Pavlov, R. V. Pisarev, and H.-J. Weber, Phys. Rev. Lett. **87**, 137202 (2001).
[56] Z. Li, Q. Liu, Y. Wang, T. Iitaka, H. Su, T. Tohyama, Z. Yang, and S. Pan, Phys. Rev. B **96**, 035205 (2017).
[57] C. Wang, X. Liu, L. Kang, B.-L. Gu, Y. Xu, and W. Duan, Phys. Rev. B **96**, 115147 (2017).
[58] M. Nakano, H. Fujita, M. Takahata, and K. Yamaguchi, J. Am. Chem. Soc. **124**, 9648 (2002).
[59] C.-K. Chan, N. H. Lindner, G. Refael, and P. A. Lee, Phys. Rev. B **95**, 041104(R) (2017).
[60] J. Rammer and H. Smith, Rev. Mod. Phys. Rev **58**, 323 (1986).
[61] W.-K. Tse and A. H. MacDonald, Phys. Rev. Lett. **105**, 057401 (2010).
[62] D. Xiao, M.-C. Chang, and Q. Niu, Rev. Mod. Phys. **82**, 1959 (2010).
[63] R. Resta, Rev. Mod. Phys. **66**, 899 (1994).
[64] E. I. Blount, in *Solid State Physics: Advances in Research and Applications*, edited by F. Seitz and D. Turnbull, Vol. 13 (Academic Press, New York, 1962).
[65] V. I. Belinicher, E. L. Ivchenko, and B. I. Sturman, Zh. Eksp. Teor. Fiz. **83**, 649 (1982).
[66] T. M. McCormick, I. Kimchi, and N. Trivedi, Phys. Rev. B **95**, 075133 (2017).